DELPHI Collaboration

DELPHI 2004-024-CONF-699
22 July, 2004

Search for excited leptons in e^+e^- collisions at $\sqrt{s} = 189 - 208$ GeV

W. Adam[1], S. Andringa[2], N. Castro[2], M.C. Espírito Santo[2], P. Gonçalves[2], C. Matteuzzi[3], A. Onofre[2], M. Pimenta[2], B. Tomé[2], F. Veloso[2]

[1] Institut für Hochenergiephysik, Österr. Akad. d. Wissensch.,
Nikolsdorfergasse 18, AT-1050 Vienna, Austria
[2] LIP,IST, Av. Elias Garcia, 14-1^o, 1, P-1000 Lisboa, Portugal
[3] Dipartimento di Fisica, Univ. di Milano-Bicocca and INFN-MILANO,
Piazza della Scienza 2, IT-20126 Milan, Italy

Abstract

A search for excited lepton production in e^+e^- collisions was performed using the data collected by the DELPHI detector at LEP at centre-of-mass energies ranging from 189 GeV to 208 GeV, corresponding to an integrated luminosity of approximately 600 pb^{-1}. No evidence for excited lepton production was found. In searches for pair-produced excited leptons lower mass limits were established, in the range 94 – 103 GeV/c^2 depending on the channel and model assumptions. In searches for singly produced excited leptons upper limits on the parameter f/Λ were established as a function of the mass. The results are preliminary.

Contributed Paper for ICHEP 2004 (Beijing)

1 Introduction

Excited leptons are expected in models with substructure in the fermionic sector. The results presented in this paper are interpreted in the context of the model described in reference [1]. There excited leptons are assumed to have spin and weak isospin equal to 1/2 and to have both their left-handed and right-handed components in weak isodoublets:

$$L_L^* = \begin{bmatrix} \nu^* \\ \ell^* \end{bmatrix}_L ; \quad L_R^* = \begin{bmatrix} \nu^* \\ \ell^* \end{bmatrix}_R$$

where ν^*, ℓ^* represent the neutral and charged excited leptons. Excited leptons ($l^* \equiv \ell^*, \nu^*$) couple to the photon and/or to the $W^{\pm}$ and Z^0 gauge bosons according to their quantum numbers and thus could be pair-produced at LEP. Single l^* production in association with their Standard Model (SM) partners ($l \equiv \ell, \nu$) is also possible but the production cross-sections depend on the ll^*V couplings, where V is a gauge boson ($V \equiv \gamma, W^{\pm}, Z^0$) [2]. Excited leptons with masses up to the centre-of-mass energy ($\sqrt{s}$) can be sought through the single production mode.

This paper presents results of a search for single and pair production of excited leptons in DELPHI at centre-of-mass energies between 189 GeV and 208 GeV. Previous results by DELPHI and other experiments can be found in references [3], [4] and [5]. The paper is organised as follows: Section 2 reviews the phenomenology of l^* production and decay and its consequences for the experimental strategy. The real and simulated data samples are presented in section 3. Event selection criteria applied to the different search channels are described in section 4 and the results obtained are presented in section 5. Finally, a summary is presented in section 6.

2 Production and decay of excited leptons

Pair production of charged excited leptons in e^+e^- collisions could proceed via s-channel γ and Z^0 exchanges, while for excited neutrinos only the Z^0 diagram contributes (figure 1). Pair production of excited electrons or excited electron neutrinos would also be possible through t-channel exchange diagrams. In this case two ll^*V vertices are involved and the contribution to the total production cross-section is expected to be negligible compared to the s-channel exchange diagrams.

Single l^* production could result from s-channel γ and Z^0 exchange (figure 1). Important additional contributions from t-channel γ and Z^0 exchange arise for excited electron production, while t-channel $W^{\pm}$ exchange can be important for the excited electron neutrino. In the t-channel production process, the SM lepton is emitted at small angles with the colliding beams direction and thus is often not detected.

The SU(2)×U(1) gauge invariant effective Lagrangian describing the magnetic transition between excited leptons and the SM leptons has the form [1]:

$$\mathscr{L}_{ll^*} = \frac{1}{2\Lambda}\overline{L^*}\sigma^{\mu\nu}\left[gf\frac{\boldsymbol{\tau}}{2}\mathbf{W}_{\mu\nu} + g'f'\frac{Y}{2}B_{\mu\nu}\right]L_L + \text{hermitian conjugate}$$

where $L^* = L_L^* + L_R^*$ and L_L is the weak isodoublet with the left-handed components of the SM leptons; $\sigma^{\mu\nu}$ is the covariant bilinear tensor, $\boldsymbol{\tau}$ are the Pauli matrices, Y is the weak hypercharge, $\mathbf{W}_{\mu\nu}$ and $B_{\mu\nu}$ represent the gauge field tensors of SU(2) and U(1) respectively, with g and g' being the corresponding Standard Model coupling constants. The parameter Λ sets the compositeness scale, with f and f' being weight factors associated with the two gauge groups. This Lagrangian is associated to the ll^*V vertex,

and describes the single production of excited leptons and their decay branching ratios. The strength of the ll^*V coupling is parameterised through f and f'. Form factors and anomalous magnetic moments of the excited leptons were not considered in the reported analyses. To reduce the number of free parameters it is usual to assume a relation between f and f', or set one of the parameters to zero. In this paper the relations $f = f'$ and $f = -f'$ were considered. With the assumption $|f| = |f'|$, the single excited lepton production cross-section depends only on the ratio f/Λ and on the excited lepton mass. The search results can also be expressed in terms of the parameter λ, which is related to the excited lepton mass (m_{l^*}) through $f/\Lambda = \sqrt{2}\lambda/m_{l^*}$.

Excited leptons with masses above 20 GeV/c^2 are assumed to decay promptly by radiating a γ, $W^{\pm}$ or Z^0 boson. Their mean lifetime is predicted to be less than 10^{-15} s in all the studied scenarios, thus for detection purposes excited leptons would essentialy decay at the production point. The decay branching ratios are also functions of the f and f' parameters. Figure 2 shows the decay branching ratios as a function of the excited lepton mass for $f = f'$ and $f = -f'$. For charged excited leptons, the electromagnetic radiative decay is forbidden if $f = -f'$ and the decays proceed exclusively through Z^0 and $W^{\pm}$ bosons. However, as long as $f \neq -f'$, there is a significant contribution to the total decay width from the electromagnetic radiative decay, even if the difference $|f| - |f'|$ is much smaller than $|f|$. If $f = f'$, the electromagnetic radiative decay branching ratio is close to 100% for m_{l^*} smaller than the $W^{\pm}$ mass (m_W), but decreases for $m_{l^*} > m_W$ reaching a value of 34% for $m_{l^*} = 200$ GeV/c^2. For excited neutrinos the electromagnetic decays are forbidden only if $f = f'$.

Many final state topologies would result from the production and decay of excited leptons. The possible final states involve isolated leptons, isolated photons, particle jets from quark fragmentation, missing energy and missing momentum.

	Final State Topologies	
Channel	Single production	Pair production
$\ell^* \to \ell\gamma$	$\ell\ell\gamma$, $(\ell)\ell\gamma$, $\ell\gamma\gamma$	$\ell\ell\gamma\gamma$
$\ell^* \to \nu W$	$jj\ell$,$jj(\ell)$	$jj\ell$,$jjjj$
$\ell^* \to \ell Z$	$jj\ell\ell$,$jj\ell(\ell)$	-
$\nu^* \to \nu\gamma$	γ	$\gamma\gamma$
$\nu^* \to \ell W$	$jj\ell$,$jj(\ell)$	$jj\ell\ell\ell$,$jj\ell\ell(\ell)$,$jjjj\ell\ell$
$\nu^* \to \nu Z$	jj	-

Table 1: Analysed final state topologies corresponding to the different production and decay modes of excited leptons. The topologies observed when the spectator or final state SM lepton is undetected are indicated with the unseen lepton in parentheses. The $\ell\gamma\gamma$ topology was considered only in the excited electron search and is expected when the spectator electron is emitted at low angle with the colliding beams.

Table 1 shows the topologies considered in the analysis, for the different l^* production and decay channels. Several of those, although not corresponding directly to the physical final state, are expected to become particularly important whenever final state particles produced with very low energy or at small angle to the colliding beams could remain undetected. For these topologies the unseen lepton is shown in parentheses.

The final states arising from the $W^{\pm}$ or Z^0 leptonic decays in the single production mode and the W^+W^- purely leptonic decays or the Z^0Z^0 final states in the pair production searches, were not considered due to their small branching ratio and/or small

signal sensitivity. In addition only the final states where both excited leptons decayed to identical gauge bosons (unmixed decays) were considered in the l^*l^* search.

Final states consisting only of single or double photons arise in the case of radiatively decaying excited neutrinos. For these topologies the results presented in [6,7] were used.

Compositeness can also be probed at LEP through the process $e^+e^- \to \gamma\gamma(\gamma)$. The additional contribution of the t-channel exchange of a virtual excited electron to the $e^+e^- \to \gamma\gamma(\gamma)$ cross-section would lead to a change on the angular distribution of the final state photons with respect to the SM prediction. This effect depends on the excited electron mass m_{e^*} and on the $ee^*\gamma$ coupling. The results presented in reference [8] were used to complement the direct searches for the excited electron in the mass region above the kinematic limit for ee^* production.

3 Detector and data samples

The data analysed were collected with the DELPHI detector in the years 1998–2000, at centre-of-mass energies ranging from 189 GeV to 208 GeV and correspond to a total integrated luminosity of 598.7 pb^{-1}. A detailed description of the DELPHI detector can be found in reference [9]. In the year 2000 the centre-of-mass energy varied from 201.5 GeV to 208.8 GeV, with an average value of $<\sqrt{s}>\simeq 206$ GeV. With the purpose of maximizing the discovery potential, these data were subdivided into centre-of-mass energy bins that were analysed independently. During the year 2000 data taking an irrecoverable failure affected one sector of the central tracking detector (TPC), corresponding to 1/12 of its acceptance. The data acquired under these conditions, approximately 60 pb^{-1}, were analysed as an independent energy bin. The luminosity weighted mean centre-of-mass energy and integrated luminosity for each analysed data set are summarised in table 2. The last column corresponds to the data taken after the TPC damage. In the remainder of the text each centre-of-mass energy bin will be referred to by the nearest integer value and the energy bin corresponding to the data taken after the TPC failure as 206*. For the double production search only the data taken in year 2000 were used in the analysis. In the single production searches the 6.9 pb^{-1} collected at $\sqrt{s} \sim 208$ GeV were analysed together with the 207 GeV data.

Year	1998	1999				2000			
$<\sqrt{s}>$ (GeV)	188.6	191.6	195.5	199.5	201.6	204.9	206.7	208.2	206.5
$\int \mathcal{L}$ (pb $^{-1}$)	151.8	25.1	76.0	82.6	40.1	79.9	77.1	6.9	59.2

Table 2: Luminosity weighted mean centre-of-mass energy and integrated luminosities for the analysed data. The last column corresponds to the data taken after the TPC damage.

Events from Standard Model processes that might contribute to the background were generated at each centre-of-mass energy using several Monte Carlo programs. $e^+e^- \to f\overline{f}(\gamma)$ events were generated with KK2F [10] (f= quark or muon), KORALZ [11] (f=tau) and BHWIDE [12] for Bhabha events (f=electron). Four-fermion final states were produced with WPHACT [13], while particular phase space regions of the $e^+e^- \to e^+e^-f\overline{f}$ process, referred to as two-photon interactions, were generated using PYTHIA [14] for hadronic final states, BDKRC [15] for $ee\mu\mu$ and $ee\tau\tau$ and BDK [16] for $eeee$ final states. $e^+e^- \to e^+e^-\gamma$ events, with one electron (positron) scattered at very

small polar angles[1] while the positron (electron) and photon have large scattering angles, usually referred to as Compton events, were generated according to [17]. The process $e^+e^- \to \gamma\gamma(\gamma)$ was simulated using the generator described in [18].

Excited lepton events were simulated to study the distributions of the relevant kinematic variables and to compute the analyses selection efficiencies. Single and pair production events of all excited lepton flavours were generated, at the relevant centre-of-mass energies and for several excited lepton masses, according to the differential cross-sections defined in reference [1]. The relation $f = f'$ was assumed for the weight factors (see section 2). In the case of single production of excited electrons, events were generated also with $f = -f'$ in order to take into account the strong dependence of the event kinematics on the relative weights of the couplings. The hadronization and decay processes were simulated using JETSET 7.4 [14]. In the single production mode, initial state radiation (ISR) was included at the event generation level. For the pair production process ISR was taken into account in the computation of the total cross-section. All the expected decay modes were included in the simulation.

The generated signal and background events were passed through the detailed simulation of the DELPHI detector and then processed with the same reconstruction and analysis programs as the real data [9]. For the data taken after the TPC failure the reconstruction algorithms for the charged particle tracks had to be adjusted. A dedicated simulation of the detector conditions after the TPC damage was also used.

4 Event selection

Topologies involving isolated leptons, isolated photons, jets and missing energy could result from the production and decay of excited leptons (see table 1).

The search for isolated particles consisted in constructing double cones centred in the direction of the charged particle tracks or of the neutral energy deposits, defined as energy deposits in the calorimeters not matched to charged particle tracks. The energy detected inside an inner cone with half opening angle of 5° was required to be above 5 GeV, while the energy contained between the inner cone and the outer cone was required to be small, to ensure isolation. Both the opening angle of the outer cone and the maximal accepted total energy contained between the two cones were allowed to vary according to the topology of the event and to the energy and identification of the reconstructed particle.

The analysis was then performed in different steps. In the first step, events with an energy greater than $0.2\sqrt{s}$ deposited above 20° in polar angle were preselected and classified in different topologies according to their multiplicity and to the number of isolated leptons and photons. In this paper, "low multiplicity" refers to events with at most five well reconstructed charged particle tracks while "high multiplicity" implies more than five such tracks. Electron, photon and muon identification were based on the standard DELPHI algorithms described in refs. [9,19]. Topology-dependent criteria were then applied, as detailed in the following subsections, and finally lepton identification was considered whenever the final state leptons could be used to tag the flavour of the excited lepton.

[1] In DELPHI a right-handed Cartesian coordinate system was used, with the z-axis pointing along the electron beam, the x-axis pointing toward the centre of the LEP ring and the origin at the centre of the detector. The polar angle θ is the angle to the electron beam direction and the azimuthal angle ϕ is the angle measured from the x-axis. In this paper the complementary value $(180° - \theta)$ is always also assumed.

4.1 Topologies with only photons

Final state topologies consisting of photons only could arise from the production of excited neutrinos decaying to a SM neutrino and a photon.

In the search for single production of excited neutrinos, events consisting of only one photon in DELPHI (single photon events) were selected. The single photon preselection followed the same strategy as described in reference [6]. The background from SM processes giving single photon events consist mainly of events with a low energy, small polar angle photon. Candidate events were thus required to have a photon with polar angle $\theta_\gamma > 45^\circ$ and with energy $\mathrm{E}_\gamma > 0.45\sqrt{s}$. In the $\nu\nu^*$ search the data from year 2000 was grouped in two bins, corresponding to $\sqrt{s} < 206$ GeV and $\sqrt{s} > 206$ GeV.

For the $\nu^*\nu^*$ search events with two photons were selected. The analysis used in the selection of two photons and missing energy described in reference [7] was followed, except for the kinematic fit imposing the Z^0 mass on the invisible system and the requirement on the missing mass.

4.2 Topologies with leptons and photons

Topologies with isolated leptons and photons are expected whenever the excited charged leptons decay by photon emission.

For the single production search the topologies $\ell\ell\gamma$, $\ell\gamma$ and $\ell\gamma\gamma$ were considered as shown in table 1. The $\ell\gamma$ topology becomes dominant for all flavours when the excited lepton mass is close to the centre-of-mass energy and the spectator SM lepton has too small an energy to be identified as an isolated particle. This topology is also crucial for the single e^* search when t-channel production dominates, in particular for the $f = f'$ scenario. The SM spectator electron would then be predominantly scattered at small polar angles and would remain undetected. Alternatively this electron could be scattered at angles covered by the STIC calorimeter, below the geometrical acceptance of the tracking detectors, and a final state topology consisting of one isolated lepton and two photon candidates would result. The $\ell\gamma\gamma$ topology was thus considered in the e^* search.

Different preselection criteria were applied, according to the event classification in each of the topologies and taking into account the relevant background processes and the specific kinematics of the signal events.

Only events with at least one photon with energy $\mathrm{E}_\gamma > 0.05\sqrt{s}$ were considered while for the lepton momentum (p_ℓ) it was required $p_\ell > 0.05\sqrt{s}$ in the topologies with only one lepton. In the $\ell\ell\gamma$ topology the sum of the two lepton momenta had to be greater that $0.1\sqrt{s}$ and the sum of the leptons and photon energies had to be greater than $0.4\sqrt{s}$. For $\ell\gamma\gamma$ events it was required that one and only one photon had a polar angle $\theta_\gamma < 9^\circ$, $p_\ell + \mathrm{E}_{\gamma_1} > 0.4\sqrt{\mathrm{s}}$ where E_{γ_1} is the energy of the low polar angle photon, and the sum of the lepton momentum and photons energies had to be greater than $0.8\sqrt{s}$. For events in the $\ell\gamma$ topology it was required that $\mathrm{E}_\gamma > 0.1\sqrt{s}$, $p_\ell > 0.1\sqrt{s}$ and $\mathrm{E}_\gamma + \mathrm{p}_\ell > 0.4\sqrt{\mathrm{s}}$.

Figure 3 shows distributions of relevant kinematic variables for each of the topologies considered, after this preselection.

Event selection was further tightened as follows. For the e^* and τ^* searches in the $\ell\gamma$ and $\ell\ell\gamma$ topologies it was required that $\theta_\gamma > 42^\circ$. For the e^* and μ^* search in $\ell\ell\gamma$, the momentum of the most energetic lepton had to be greater than $0.05\sqrt{s}$. The background from Bhabha scattering events in the $\ell\ell\gamma$ topology was reduced by requiring $\mathrm{E}_\gamma \cdot \sin\alpha > 0.08\sqrt{s}$, where E_γ is the photon energy and α is the angle between the photon direction and the direction of the nearest particle. In the $\ell\gamma\gamma$ topology one photon had to be detected above 25° in polar angle.

For the pair production search the $\ell\ell\gamma\gamma$ topology was considered. The expected background is rather low and simpler cuts were applied. Both leptons were required to have a momentum above 10 GeV/c. Events were kept as candidates if a lepton-photon pairing could be found for which the difference between the invariant masses of the two lepton-photon pairs was smaller than 15 GeV/c^2 in the e^* and μ^* searches and less than 20 GeV/c^2 in the τ^* search.

The excited lepton mass can be reconstructed by computing the lepton-photon invariant mass. In the $\ell\gamma\gamma$ topology the relevant photon is the one detected at high polar angle, while in the $\ell\ell\gamma$ topology the two possible lepton-photon pairings were considered. The invariant mass resolution was improved by rescaling the measured energies or momenta. This was done imposing energy-momentum conservation and using just the polar and azimuthal angles, which are well measured in the detector (angular precisions of ± 1.7 mrad in ϕ and ± 1 mrad in θ are obtained for high energy photons and of about ± 1 mrad or better in θ and ϕ for high momentum charged particle tracks, in the central part of the DELPHI detector [9]). In order to take into account the energy lost through initial state radiation, the rescaling was also applied assuming the presence of an additional photon along the beam direction. This procedure accounts also for the case when the spectator electron is lost in the beam pipe. The compatibility of the rescaled and the measured values was quantified through the variable χ^2, defined as:

$$\chi^2 \;=\; \frac{1}{n}\sum_{i=1,n}\left(\frac{p_i^{calc}-p_i^{meas}}{\sigma_i}\right)^2$$

where n is the number of measured particles, p_i^{meas} are the measured momenta or energies and p_i^{calc} are the values calculated from the kinematic constraint. The quadratic sum of the errors on p_i^{calc} and p_i^{meas}, σ_i, is defined in reference [3]. The χ^2 was computed separately for charged particles ($\chi^2_{charged}$) and photons ($\chi^2_{photons}$). The result from the rescaling assuming an additional particle along the beam direction was retained whenever it yielded a smaller total χ^2. In any case only events with $\min(\chi^2_{\rm charged},\chi^2_{\rm photons}) < 5$ were selected. The resolution on the lepton-photon invariant mass, after applying the kinematic constraints, was found to be in the range 0.2-0.6 GeV/c^2 for electrons and muons, and 1.5-2.0 GeV/c^2 for taus.

Finally, events were considered as candidates in the e^* search if all leptons were identified as electrons, and in the μ^* channel if the most energetic lepton was identified as a muon and no particle was identified as an electron. In the τ^* search, a difference between the measured and rescaled momenta of the leptons, characteristic of the presence of neutrinos from tau decays, was required by imposing $\chi^2_{charged} > 5$ ($\chi^2_{charged} > 10$ in the $\ell\ell\gamma\gamma$ topology).

4.3 Topologies with jets and leptons

4.3.1 Single production analysis

Final state topologies with jets and isolated leptons were considered in the search for excited leptons decaying to $\mathrm{W}^\pm$ or Z^0 ($\ell^* \to \nu\mathrm{W}$, $\ell^* \to \ell\mathrm{Z}^0$, $\nu^* \to \ell\mathrm{W}$ and $\nu^* \to \nu\mathrm{Z}^0$). Only the final states arising from the hadronic decays of the $\mathrm{W}^\pm$ and Z^0 bosons were studied. Depending on the search channel, up to two isolated leptons could be present. The relevant topologies considered in the single production search were thus jj, $jj\ell$ and $jj\ell\ell$. All particles in the event, excluding the isolated leptons, were clustered into jets using the Durham algorithm [20]. Two-jet events were selected by requiring the Durham

resolution variable in the transition from three to two jets, $y_{(3\to2)}$, to be lower than 0.06 and from two to one jet, $y_{(2\to1)}$, to be greater than 0.01. The polar angle of isolated leptons had to be above 25°.

For excited lepton masses not excluded by previous searches, the gauge bosons are produced on-shell and the invariant mass of the two jets (M_{jj}) should be compatible with a $W^{\pm}$ or Z^0 boson. The loose condition $40 < M_{jj} < 120$ GeV/c^2 was thus applied in all topologies.

In addition, since the gauge bosons originating from excited lepton decays are not at rest, the two jets are also expected to be acoplanar – the jet-jet acoplanarity (A^{jj}_{cop}) was defined as $180° - \Phi$, Φ being the angle between the projections of the jet momenta in the plane perpendicular to the beam.

Background events in the $jj\ell$ topology come mainly from the production of W^+W^- pairs, with one boson decaying to quarks and the other to a charged lepton and a neutrino ($W^{\pm}$ semileptonic decays). The quantity $\xi = Q_W \cdot \cos\theta_W$, Q_W and θ_W being the boson charge and polar angle respectively, was used to discriminate signal events against the W^+W^- background. In $W^{\pm}$ semileptonic decays Q_W was given by the lepton charge (Q_ℓ) and θ_W was estimated, neglecting radiation effects, from the jet directions as $180° - \theta_{\not\jmath}$, where $\theta_{\not\jmath}$ is the polar angle of the sum of the momenta of the two jets after the kinematic fit described below.

Figure 4 shows the distributions for the jet-jet acoplanarity, the variable ξ for events with the lepton charge unambiguously determined and the energy of the most energetic lepton, for the jj, $jj\ell$ and $jj\ell\ell$ topologies, after these preselection cuts. The different topology dependent selection criteria are described in the following paragraphs.

In jj events the main background comes from $e^+e^- \to q\overline{q}(\gamma)$ events, where the photon is emitted at a very small polar angle or is soft, and thus remains undetected. Since the transverse momentum of the photon is always very small (typically < 2 GeV/c at $\sqrt{s} = 200$ GeV), this process results in two jets with small acoplanarity. Candidate events were required to have $A^{jj}_{cop} > 25°$ and the polar angle of both jets had to be larger than 20°.

A looser acoplanarity cut, $A^{jj}_{cop} > 10°$, was applied in the $jj\ell$ topology. The $W^{\pm}$ bosons in background events are produced preferentially in the forward direction and ξ is peaked towards -1. To reject the W^+W^- background further candidate events with the lepton charge unambiguously determined were required to satisfy also $\xi > -0.6$.

In the $jj\ell\ell$ topology the angle between the two lepton directions or between any of the leptons and the jet directions had to be greater than 10°. No acoplanarity cut was applied.

In order to improve the estimation of the jet momenta and energies a kinematic constrained fit [21] was applied to the selected events. Events in the jj and $jj\ell$ topologies can arise from excited lepton decays mediated by a $W^{\pm}$ or Z^0 boson (see table 1) and thus the invariant mass of the jet-jet system was constrained to be either m_W or m_Z, depending on the search channel. For events in the $jj\ell\ell$ topology the fit was performed imposing only m_Z. Only events with a χ^2 per degree of freedom lower than 5 were retained.

The excited lepton mass has been estimated in several of the topologies considered. The relevant variables used were the jet-jet-lepton ($\nu\nu^* \to \nu\ell W^{\pm}$) and jet-jet-neutrino ($\ell\ell^* \to \ell\nu W^{\pm}$) invariant masses, and the recoil mass of isolated leptons ($\ell\ell^* \to \ell\nu W^{\pm}$, $\ell\ell^* \to \ell\ell Z^0$). The resolution on the jet-jet-neutrino invariant mass was found to vary between 1 GeV/c^2 and 5 GeV/c^2. In the $\tau\tau^* \to \tau\nu W^{\pm}$ channel, the τ^* mass was reconstructed only for signal masses $m_{\tau^*} > 0.9\sqrt{s}$ and was obtained from the recoil mass of the spectator lepton; the resolution ranged between 3 GeV/c^2 and 6 GeV/c^2. The resolution

on the jet-jet-lepton invariant mass was about 2 GeV/c^2 for $m_{\nu^*} = 100$ GeV/c^2, increasing to about 10 GeV/c^2 for $m_{\nu^*} = 200$ GeV/c^2; no mass reconstruction was attempted in the ν_τ^* channel.

In the last step of the analysis, the various excited lepton production and decay modes within the same topology were treated differently. In the search for excited leptons of the first or second family, the final state SM charged leptons identification had to match the excited lepton flavour. In the case of the $\tau^* \to \tau \mathrm{Z}^0$ search the lepton energy had to be lower than $0.3\sqrt{s}$ for events in the $jj\ell$ topology, while in $jj\ell\ell$ events at least one lepton with energy lower than $0.2\sqrt{s}$ was required. In $\nu_\tau^* \to \tau \mathrm{W}^\pm$ events, the lepton energy had to be lower than $0.2\sqrt{s}$.

4.3.2 Pair production analysis

$\nu^*\nu^*$ search

In the search for pair production of neutral excited leptons decaying to W$^\pm$ bosons ($\nu^*\nu^* \to \ell\mathrm{W}\ell\mathrm{W}$) only the fully hadronic and semileptonic decays of W$^+$W$^-$ pairs were taken into account. The final state topologies consist of the W$^+$W$^-$ decay products (two jets and one lepton or four jets) and of two additional charged leptons, yielding a clear signature. The background is mainly due to Z^{0}Z^0 events.

Multijet events were selected requiring $y_{(2\to1)} > 0.03$. Events with at least two isolated leptons were kept. If exactly two isolated leptons were found it was further required that $y_{(3\to2)} > 0.01$.

In the search for ν_e^* and ν_μ^* , the final state had to contain at least two charged leptons of the corresponding flavour. For the ν_τ^* search the missing energy was required to be greater than $0.1\sqrt{s}$.

$\ell^*\ell^*$ search

The final state topologies considered in the search for pair production of charged excited leptons decaying to W$^\pm$ bosons ($\ell^*\ell^* \to \nu\mathrm{W}\nu\mathrm{W}$) were four jets or two jets and one lepton, resulting respectively from the fully hadronic or semileptonic decays of the W$^+$W$^-$ pair.

Contrary to the $\nu^*\nu^*$ search described above, the two additional leptons in the final state are now neutrinos, seen as missing energy. Signal events have thus a signature very similar to the W$^+$W$^-$ background events. In order to boost the small differences between the signal and background kinematics a discriminant analysis was used in the $\ell^*\ell^* \to \nu\mathrm{W}\nu\mathrm{W}$ search. After the event preselection a signal likelihood $\mathcal{L}_S$ and a background likelihood $\mathcal{L}_B$ were constructed as the product of probability density functions (PDFs) of relevant kinematic variables, as described below. The discriminant variable was defined as $\mathcal{L}_S/\mathcal{L}_B$.

The semileptonic and the fully hadronic cases were treated separately. In the semileptonic analysis, events with no isolated photons and at least one isolated lepton were considered. The remaining particles in the event were clustered into jets. Two-jet events were selected by requiring that the Durham resolution variables satisfied the criteria $y_{(3\to2)} < 0.06$ and $y_{(2\to1)} > 0.01$. The background from $e^+e^- \to q\overline{q}(\gamma)$ events was reduced by requiring the polar angle of the direction of the missing momentum to be above 20°. The minimum transverse momentum of the lepton with respect to any of the jets had to be greater than 10 GeV/c; the lepton polar angle was required to be above 20° for muons and above 40° for electrons. The following variables were then used to build the discriminant variable:

- missing energy of the event,
- angle between the two jets,
- energy of the lepton,
- angle between the lepton and missing momentum directions,
- $Q_\ell \cdot \cos\theta_\ell$, where Q_ℓ and θ_ℓ are the charge and polar angle of the lepton.

In the fully hadronic analysis it was required that no isolated photons or leptons were present. Four jet events were selected by requiring $y_{(4\to3)} > 0.003$ and $y_{(3\to2)} > 0.03$. The jets were assigned to each of the $W^\pm$ bosons by choosing the pairing that minimized the sum of the squares of the differences between the jet-jet invariant masses and the $W^\pm$ mass. A fit imposing energy-momentum conservation and constraining the invariant mass of the two jet pairs to the $W^\pm$ mass was performed. The following quantities were then used to build the discriminant variable:

- missing energy of the event,
- the angle between the directions of the two jets in each jet-jet pairing,
- angle between the directions of the two reconstructed W bosons.

Distributions of variables used in the discriminant step of the analysis are shown in figure 5. A good agreement with SM predictions is observed.

5 Results

For a given excited lepton production and decay mode several final state topologies might contribute (see table 1). The relevance of each topology depends on the decay branching ratios, which are a function of the excited lepton mass and of the coupling parameters.

The number of excited lepton candidates found in the single and pair production searches at the various centre-of-mass energies, together with the expected background from SM processes, are summarized in tables 3 and 4, for the different l^* types and decay modes. These numbers were obtained by adding the results from the different exclusive topologies considered in each l^* decay (as listed in table 1). In many cases there are candidate events common to the different l^* searches (e.g. the events selected in the jj topology are candidates to all $\ell^* \to \nu W$ searches, independently of the ℓ^* flavour), but in each l^* search there are no common candidates selected in different search channels.

The signal selection efficiencies for all the studied channels, at $\sqrt{s} = 206$ GeV, are given in table 5, for specific excited lepton mass values. The dependence of the efficiency on the excited lepton mass is weak, due to the combination of selections in several topologies which are sensitive to different mass regions.

Figures 6 and 7 show the invariant mass distributions for the candidates selected in the various single production searches, obtained by adding the data from all the analysed centre-of-mass energies and topologies considered. In figure 8 are shown the distributions for the discriminant variables used in the double production search, for both the semileptonic and the hadronic final states.

5.1 Systematic uncertainties

Systematic uncertainties affect both the background and the signal efficiency estimations.

At the event generation level, errors on the computed cross-sections translate into uncertainties on the expected number of background events. The overall error on the

number of background events resulting from the systematic errors on the cross-section of processes contributing significantly to the background is typically less than 2% [22].

The simulated distributions of the kinematic variables used in the event selection may not match the distributions for the real data, due either to a not perfect description of the detector or of the background processes at the event generation level. Possible effects on the selected number of simulated events were estimated by studying the change in the ratio between the number of selected events in the data and simulated background, when varying each selection cut around the chosen value, keeping the other cuts fixed. In each topology the contributions from the different selection cuts were added in quadrature. Values ranging from 5% to 8%, depending on the topology considered, were obtained. These were taken as an estimate of the contribution from the analysis cuts to the systematic error on the background expectation. For each final state topology the systematic uncertainties to the signal selection efficiencies due to the selection cuts were assumed to be equal to and fully correlated with the background error.

The statistical errors on the background and signal efficiencies were taken as uncorrelated systematic uncertainties.

An additional source of systematic error on the signal efficiency is due to the description of initial state radiation (ISR) effects at the event generator level. ll^* events were generated with collinear ISR only. As long as ISR photons were emitted below the DELPHI acceptance, this would result only in a small change on the event kinematics, with low impact on the signal selection efficiency. However, if the ISR photon was detected, the event topology would be different from the topologies considered in the analysis, resulting in a smaller efficiency for the signal. This effect was estimated using $e^+e^- \to e^+e^-$ and $e^+e^- \to \mu^+\mu^-$ simulated events at various centre-of-mass energies. An average correction factor of 0.9 was obtained and was used to rescale the selection efficiencies. The spread on the corrections obtained at the different centre-of-mass energies, of the order of 2%, was taken as an independent contribution to the systematic error of the signal efficiencies.

The systematic uncertainties discussed in this section were included in the computation of the exclusion limits.

5.2 Limits

Limits at 95% confidence level (CL) were computed using the likelihood ratio method described in reference [23]. This method is well suited both for the combination of different search channels and for the inclusion of mass information. Searches in each topology at each centre-of-mass energy were treated as independent channels. Whenever the mass of the particle being searched for could be reconstructed, the PDF for a given signal mass hypothesis was assumed to be Gaussian with mean value equal to the tested signal mass and standard deviation equal to the signal mass resolution. For channels where the l^* mass was not reconstructed, all selected events were candidates for all signal mass hypotheses. For the $\ell^*\ell^* \to \nu\mathrm{W}\nu\mathrm{W}$ channel, for which a discriminant analysis was performed, the PDFs of the likelihood ratio obtained at each signal mass hypothesis were used.

From the single production search results, upper limits on the production cross-section multiplied by the decay branching ratio ($\sigma \times \mathrm{BR}$), as a function of the mass, were derived for each l^* flavour and decay mode ($\gamma, \mathrm{W}^\pm, \mathrm{Z}^0$). These limits are shown in figure 9. As already discussed, the kinematics of single e^* production is sensitive to the contribution from t-channel γ exchange, with impact on the selection efficiencies. Since the $\ell\ell^*\gamma$ coupling becomes significant even for a slight departure from the $f = -f'$ scenario, the

e^* limits were computed using the selection efficiencies obtained with $f = f'$. For the other l^* flavours the selection efficiencies do not depend on the f and f' assignments. The limits on $\sigma \times$ BR can thus be interpreted in broader compositeness scenarios.

The cross-section for single l^* production is a function not only of the mass of the particle but also of the coupling parameter f/Λ, while the pair production cross-section is a function of the excited lepton mass only. Upper limits on f/Λ as a function of m_{l^*} and lower limits on m_{l^*} were derived from the single and pair production searches respectively, by combining the search results in the various l^* decay modes. The dependence of the decay BR's and production cross-sections on the l^* mass as given in reference [1] were assumed. The production cross-sections were computed taking into account initial state radiation effects.

Figures 10 and 11 show the limits on f/Λ as a function of m_{l^*} for $f = f'$ and $f = -f'$, respectively. The lower limits on the excited lepton masses are given in table 6 for the two scenarios. Figure 12 shows the upper limit on f/Λ for the single production of excited electrons with $f = f'$, obtained by taking the best limit of the direct search results (figure 10(a)) and the indirect result from the search for deviations in the $e^+e^- \to \gamma\gamma(\gamma)$ differential cross-section [8]. Thus the exclusion of the model parameters can be extended beyond the kinematic limit.

6 Summary

The data collected by DELPHI at $\sqrt{s} = 189-208$ GeV, corresponding to an integrated luminosity of 598.7 pb^{-1}, were analysed to search for excited leptons decaying promptly through γ, Z^0 or $W^\pm$ emission. No evidence for excited lepton production was observed.

The search for l^* pair production resulted in the mass limits quoted in table 6. These are close to the kinematic limit for all charged (neutral) excited leptons in the $f = f'$ ($f = -f'$) scenario. The single production search gave the limits on f/Λ shown in Figures 10, 11 and 12. Model independent upper bounds on $\sigma \times$ BR were also derived for each lepton type and decay channel, thus allowing for new interpretations in broader compositeness scenarios. These results confirm and extend the limits set previously at LEP and HERA [4,5].

Acknowledgements

We are greatly indebted to our technical collaborators, to the members of the CERN-SL Division for the excellent performance of the LEP collider, and to the funding agencies for their support in building and operating the DELPHI detector.
We acknowledge in particular the support of
Austrian Federal Ministry of Education, Science and Culture, GZ 616.364/2-III/2a/98,
FNRS–FWO, Flanders Institute to encourage scientific and technological research in the industry (IWT), Belgium,
FINEP, CNPq, CAPES, FUJB and FAPERJ, Brazil,
Czech Ministry of Industry and Trade, GA CR 202/99/1362,
Commission of the European Communities (DG XII),
Direction des Sciences de la Matière, CEA, France,
Bundesministerium für Bildung, Wissenschaft, Forschung und Technologie, Germany,
General Secretariat for Research and Technology, Greece,
National Science Foundation (NWO) and Foundation for Research on Matter (FOM), The Netherlands,
Norwegian Research Council,
State Committee for Scientific Research, Poland, SPUB-M/CERN/PO3/DZ296/2000, SPUB-M/CERN/PO3/DZ297/2000 and 2P03B 104 19.
JNICT–Junta Nacional de Investigação Científica e Tecnológica, Portugal,
Vedecka grantova agentura MS SR, Slovakia, Nr. 95/5195/134,
Ministry of Science and Technology of the Republic of Slovenia,
CICYT, Spain, AEN99-0950 and AEN99-0761,
The Swedish Natural Science Research Council,
Particle Physics and Astronomy Research Council, UK,
Department of Energy, USA, DE–FG02–94ER40817.

References

[1] K. Hagiwara, D. Zeppenfeld and S. Komamiya, Zeit. Phys. **C29** (1985) 115;
F. Boudjema, A. Djouadi and J.L. Kneur, Zeit. Phys. **C57** (1993) 425.
[2] A. Djouadi, Zeit. Phys. **C63** (1994) 317.
[3] DELPHI Coll., P. Abreu et al., Phys. Lett. **B380** (1996) 480.
[4] DELPHI Coll., P. Abreu et al., Eur. Phys. J. **C8** (1999) 41;
[5] ALEPH Coll., T. Medcalf et al., "Search for excited leptons in e+e- collisions at $\sqrt{s} = 188.6$ GeV", CERN-OPEN 99-171, contributed paper to EPS-HEP99;
L3 Coll., P. Achard et al., Phys. Lett. **B568** (2003) 23;
L3 Coll., M. Acciarri et al., Phys. Lett. **B502** (2001) 37;
OPAL Coll., G. Abbiendi et al., Phys. Lett. **B544** (2002) 57;
OPAL Coll., G. Abbiendi et al., Eur. Phys. J. **C14** (2000) 73;
H1 Coll., C. Adloff et al., Phys. Lett. **B548** (2002) 35;
H1 Coll., C. Adloff et al., Phys. Lett. **B525** (2002) 9;
H1 Coll., C. Adloff et al., Eur. Phys. J. **C17** (2000) 567;
ZEUS Coll., S. Chekanov et al., Phys. Lett. **B549**(2002)32
ZEUS Coll., J. Breitweg et al., Zeit. Phys. **C76** (1997) 631.
[6] DELPHI Coll., J. Abdallah et al., "Photon Events with Missing Energy in e^+e^- Collisions at $\sqrt{(}s) = 130$ to 209 GeV", CERN-EP/2003-093 (Submitted to Euro.

Phys. J. C).
[7] DELPHI Coll., J. Abdallah et al., Eur. Phys. J. **C35** (2004) 313.
[8] DELPHI Coll., J. Abdallah et al., "Determination of the $e^+e^- \to \gamma\gamma(\gamma)$ cross-section at LEP 2", CERN-PH-EP/2004-017 (Submitted to Euro. Phys. J.).
[9] DELPHI Coll., P. Aarnio et al., Nucl. Instr. Methods **A303** (1991) 233;
DELPHI Coll., P. Abreu et al., Nucl. Instr. Methods **A378** (1996) 57.
[10] S. Jadach, B.F.L. Ward and Z. Wąs, Comp. Phys. Comm. **130** (2000) 260.
[11] S. Jadach, B.F.L. Ward and Z. Wąs, Comp. Phys. Comm. **66** (1991) 276.
[12] S. Jadach, W. Placzek and B.F.L. Ward, Phys. Lett. **B390** (1997) 298.
[13] E. Accomando and A. Ballestrero, Comp. Phys. Comm. **99** (1997) 270;
E. Accomando, A. Ballestrero and E. Maina, Comp. Phys. Comm. **150** (2003)166.
[14] T. Sjöstrand et al., Comp. Phys. Comm. **135** (2001) 238;
T. Sjöstrand, Comp. Phys. Comm. **82** (1994) 74;
T. Sjöstrand, Pythia 5.7 and Jetset 7.4, CERN-TH/7112-93.
[15] F.A. Berends, P.H. Daverveldt and R. Kleiss, Comp. Phys. Comm. **40** (1986) 271.
[16] F.A. Berends, P.H. Daverveldt and R. Kleiss, Comp. Phys. Comm. **40** (1986) 285.
[17] D. Karlen, Nucl. Phys. **B289** (1987) 23.
[18] F. Berends and R. Kleiss, Nucl. Phys. **B186** (1981) 22.
[19] F.Cossutti et al., "REMCLU : a package for the Reconstruction of Electromagnetic CLUsters at LEP200", DELPHI Note 2000-164 PROG 242.
[20] S. Catani et al., Phys. Lett. **B269** (1991) 432.
[21] DELPHI Coll., P. Abreu et al., Eur. Phys. J. **C2** (1998) 581.
[22] CERN Report 96-01, vol.2 (1996), "Workshop on Physics at LEP2", edited by G. Altarelli, T. Sjöstrand and F.Zwirner.
CERN Report 2000-009 (2000), "LEP2 Monte Carlo Workshop: Report of the Working Groups on Precision Calculations for LEP2 Physics", edited by S. Jadach, G. Passarino and R. Pittau.
[23] A. L. Read, CERN Report 2000-005, p.81 (2000), "Workshop on Confidence Limits", edited by F. James, L. Lyons and Y. Perrin.

$\sqrt{s}$ (GeV)	Channel	Excited lepton flavour					
		e		μ		τ	
189	$\ell^* \to \ell\gamma$	366	(408.2±6.7)	39	(44.0±1.5)	62	(54.3±2.7)
	$\ell^* \to \nu W^\pm$	202	(217.6±4.8)	195	(195.5±4.3)	432	(447.8±7.1)
	$\ell^* \to \ell Z^0$	51	(42.0±3.4)	8	(10.00±0.66)	55	(40.9±2.7)
	$\nu^* \to \nu\gamma$	3 (0.70±0.17)					
	$\nu^* \to \ell W^\pm$	175	(180.1±4.9)	133	(131.3±3.2)	203	(196.5±4.9)
	$\nu^* \to \nu Z^0$	75 (81.1±3.1)					
192	$\ell^* \to \ell\gamma$	61	(66.4±2.0)	8	(7.29±0.27)	10	(8.05±0.76)
	$\ell^* \to \nu W^\pm$	28	(38.04±0.79)	25	(33.71±0.69)	56	(75.2±1.1)
	$\ell^* \to \ell Z^0$	5	(5.24±0.44)	1	(2.01±0.16)	3	(6.56±0.43)
	$\nu^* \to \nu\gamma$	0 (0.10±0.03)					
	$\nu^* \to \ell W^\pm$	24	(28.53±0.75)	18	(22.01±0.53)	26	(31.33±0.79)
	$\nu^* \to \nu Z^0$	9 (14.87±0.49)					
196	$\ell^* \to \ell\gamma$	201	(188.9±3.3)	18	(20.27±0.73)	24	(23.4±1.3)
	$\ell^* \to \nu W^\pm$	108	(117.3±2.4)	103	(101.6±2.1)	232	(230.0±3.5)
	$\ell^* \to \ell Z^0$	26	(20.4±1.5)	3	(5.81±0.36)	23	(21.0±1.2)
	$\nu^* \to \nu\gamma$	2 (0.70±0.08)					
	$\nu^* \to \ell W^\pm$	90	(91.2±2.3)	72	(64.6±1.6)	106	(96.7±2.4)
	$\nu^* \to \nu Z^0$	38 (45.6±1.5)					
200	$\ell^* \to \ell\gamma$	190	(198.8±3.5)	25	(20.74±0.74)	26	(27.3±1.3)
	$\ell^* \to \nu W^\pm$	128	(131.1±2.6)	102	(114.6±2.4)	239	(248.0±3.7)
	$\ell^* \to \ell Z^0$	29	(19.3±1.4)	9	(7.05±0.48)	28	(22.4±1.3)
	$\nu^* \to \nu\gamma$	6 (1.7±0.1)					
	$\nu^* \to \ell W^\pm$	116	(96.7±2.4)	70	(70.5±1.7)	108	(102.5±2.5)
	$\nu^* \to \nu Z^0$	42 (52.2±1.7)					
202	$\ell^* \to \ell\gamma$	87	(94.9±2.1)	8	(9.44±0.38)	16	(12.05±0.73)
	$\ell^* \to \nu W^\pm$	79	(61.9±1.2)	54	(54.1±1.1)	138	(119.6±1.8)
	$\ell^* \to \ell Z^0$	5	(10.53±0.77)	4	(3.45±0.25)	9	(11.42±0.68)
	$\nu^* \to \nu\gamma$	1 (1.2±0.1)					
	$\nu^* \to \ell W^\pm$	54	(46.8±1.2)	28	(33.57±0.84)	55	(51.4±1.3)
	$\nu^* \to \nu Z^0$	31 (24.91±0.80)					
205	$\ell^* \to \ell\gamma$	179	(182.7±3.8)	20	(18.28±0.34)	27	(24.3±1.2)
	$\ell^* \to \nu W^\pm$	119	(123.8±2.4)	94	(102.4±2.1)	225	(231.5±3.4)
	$\ell^* \to \ell Z^0$	22	(18.0±1.3)	7	(6.82±0.47)	24	(21.5±1.3)
	$\nu^* \to \nu\gamma$	5 (1.3±0.2)					
	$\nu^* \to \ell W^\pm$	98	(90.9±2.3)	60	(61.8±1.6)	88	(100.1±2.4)
	$\nu^* \to \nu Z^0$	46 (50.5±1.6)					
206*	$\ell^* \to \ell\gamma$	120	(129.8±2.7)	11	(13.15±0.25)	16	(19.2±1.0)
	$\ell^* \to \nu W^\pm$	79	(93.9±1.8)	70	(79.8±1.7)	138	(173.1±2.5)
	$\ell^* \to \ell Z^0$	15	(14.3±1.0)	3	(4.51±0.35)	16	(14.75±0.88)
	$\nu^* \to \ell W^\pm$	58	(67.4±1.7)	41	(46.4±1.2)	53	(72.3±1.7)
	$\nu^* \to \nu Z^0$	37 (38.9±1.2)					
> 206	$\nu^* \to \nu\gamma$	1 (2.6±0.2)					
207 + 208	$\ell^* \to \ell\gamma$	172	(180.9±3.3)	15	(18.28±0.34)	21	(25.1±1.2)
	$\ell^* \to \nu W^\pm$	110	(130.6±2.5)	94	(110.7±2.3)	205	(239.3±3.5)
	$\ell^* \to \ell Z^0$	30	(22.8±1.6)	6	(6.9±0.5)	21	(23.4±1.3)
	$\nu^* \to \ell W^\pm$	86	(96.4±2.4)	52	(64.9±1.7)	87	(99.9±2.4)
	$\nu^* \to \nu Z^0$	53 (55.3±1.7)					

Table 3: Number of candidates for the different excited lepton decay channels in the single production search. The numbers in parentheses correspond to the SM background expectations with the statistical errors.

$\sqrt{s}$ (GeV)	Channel	Excited lepton flavour		
		e	μ	τ
205	$\ell^* \to \ell\gamma$	0 (1.25±0.33)	0 (0.38±0.05)	1 (2.57±0.41)
	$\nu^* \to \nu\gamma$	4 (3.26±0.33)		
	$\ell^* \to \nu W$ (hadr.)	403 (419.9±5.1)		
	$\ell^* \to \nu W$ (semilep.)	261 (231.1±3.1)		
	$\nu^* \to \ell W$	1 (3.21±0.33)	1 (0.99±0.16)	18 (17.43±0.87)
206*	$\ell^* \to \ell\gamma$	1 (0.52±0.20)	0 (0.29±0.04)	3 (1.48±0.27)
	$\nu^* \to \nu\gamma$	6 (2.21±0.26)		
	$\ell^* \to \nu W$ (hadr.)	280 (311.0±3.8)		
	$\ell^* \to \nu W$ (semilep.)	154 (176.6±2.4)		
	$\nu^* \to \ell W$	6 (2.56±0.32)	0 (0.93±0.14)	15 (12.04±0.61)
207	$\ell^* \to \ell\gamma$	1 (1.49±0.34)	2 (0.41±0.05)	3 (2.59±0.39)
	$\nu^* \to \nu\gamma$	3 (3.50±0.36)		
	$\ell^* \to \nu W$ (hadr.)	408 (416.9±5.0)		
	$\ell^* \to \nu W$ (semilep.)	228 (239.0±3.2)		
	$\nu^* \to \ell W$	3 (3.10±0.32)	1 (1.74±0.22)	20 (17.22±0.89)
208	$\ell^* \to \ell\gamma$	0 (0.16±0.06)	0 (0.04±0.01)	0 (0.25±0.07)
	$\nu^* \to \nu\gamma$	-		
	$\ell^* \to \nu W$ (hadr.)	34 (34.95±0.85)		
	$\ell^* \to \nu W$ (semilep.)	10 (19.94±0.54)		
	$\nu^* \to \ell W$	0 (0.36±0.08)	0 (0.10±0.02)	2 (1.68±0.17)

Table 4: Number of excited lepton candidates for the different decay channels and the different centre-of-mass energies in the pair production search. The numbers in parentheses correspond to the SM background expectations with the statistical errors.

channel	Excited lepton flavour		
	e	μ	τ
Single production			
$\ell^* \to \ell\gamma$	40.3±2.0	61.2±2.5	22.5±1.5
$\ell^* \to \nu W$	33.1±1.8	32.9±1.8	43.3±2.1
$\ell^* \to \ell Z$	19.7±1.4	41.7±2.0	19.6±1.4
$\nu^* \to \nu\gamma$	32.5±1.8		
$\nu^* \to \ell W$	34.1±1.8	34.2±1.8	18.0±1.3
$\nu^* \to \nu Z$	40.7±2.0		
Pair production			
$\ell^* \to \ell\gamma$	38.2 ±1.4	50.8 ±1.6	17.5 ±0.9
$\ell^* \to \nu W$ (hadr.)	22.1±0.7		
$\ell^* \to \nu W$ (semilep.)	16.3±0.6		
$\nu^* \to \nu\gamma$	52.9±2.3		
$\nu^* \to \ell W$	27.9±1.7	42.3±2.1	13.1±1.1

Table 5: Selection efficiencies (in %) for the different excited lepton flavours and decay channels, in the single (top) and pair (bottom) production modes. Efficiencies are quoted for excited lepton masses of m_{l^*}=200 GeV/c^2 in the single production and m_{l^*}=100 GeV/c^2 in the pair production, at $\sqrt{s}$ =206 GeV.

	e^*	μ^*	τ^*		ν_e^*	ν_μ^*	ν_τ^*
$f = f'$	103.1	103.2	102.7	$f = f'$	101.9	103.2	94.2
$f = -f'$	101.0	101.0	101.0	$f = -f'$	101.9	102.2	101.9

Table 6: Lower limits (in GeV/c^2) at 95 % CL on the excited lepton masses obtained from the pair production searches.

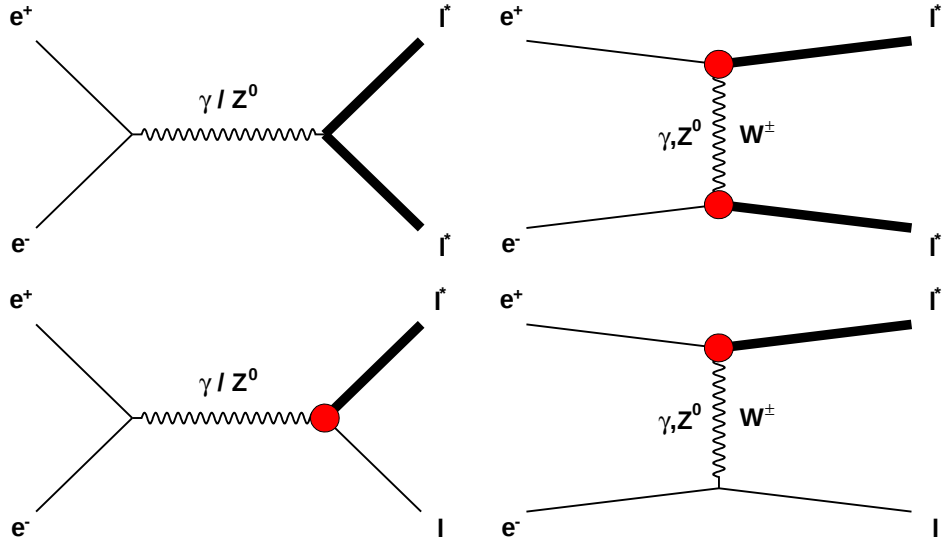

Figure 1: Feynman diagrams for the double (top) and single (bottom) excited lepton production. Each l^* is shown as a thicker line. The vertex shown as a closed circle represents a ll^*V coupling ($V \equiv \gamma, \mathrm{W}^\pm, \mathrm{Z}^0$) proportional to $1/\Lambda$.

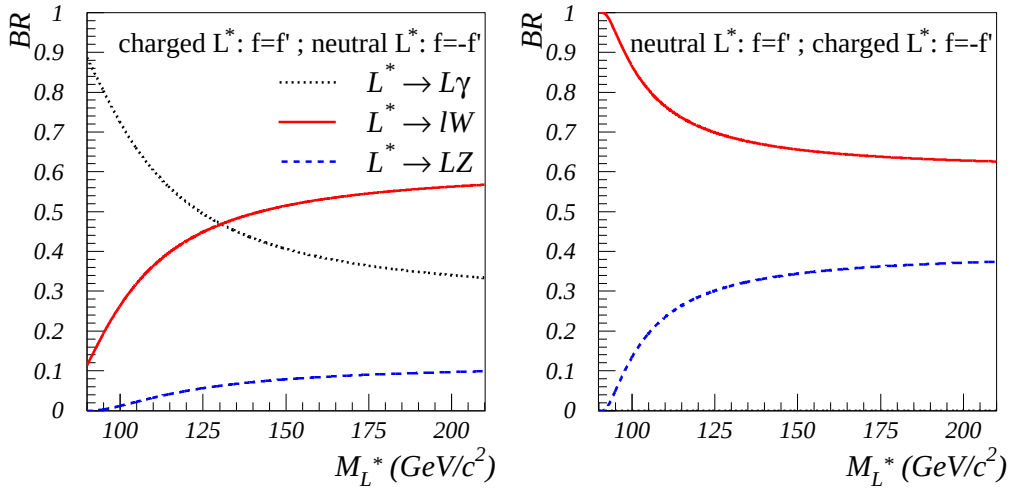

Figure 2: Branching ratios of the excited lepton (L*) decays as a function of the mass. L represents the SM lepton of the same flavour as L*, while ℓ stands for the SM lepton with electric charge differing by one unit from the L* charge. In the left plot are shown the branching ratios for charged (neutral) leptons when $f = f'$ ($f = -f'$). As shown in the right plot the electromagnetic decay is forbidden for neutral (charged) leptons when $f = f'$ ($f = -f'$).

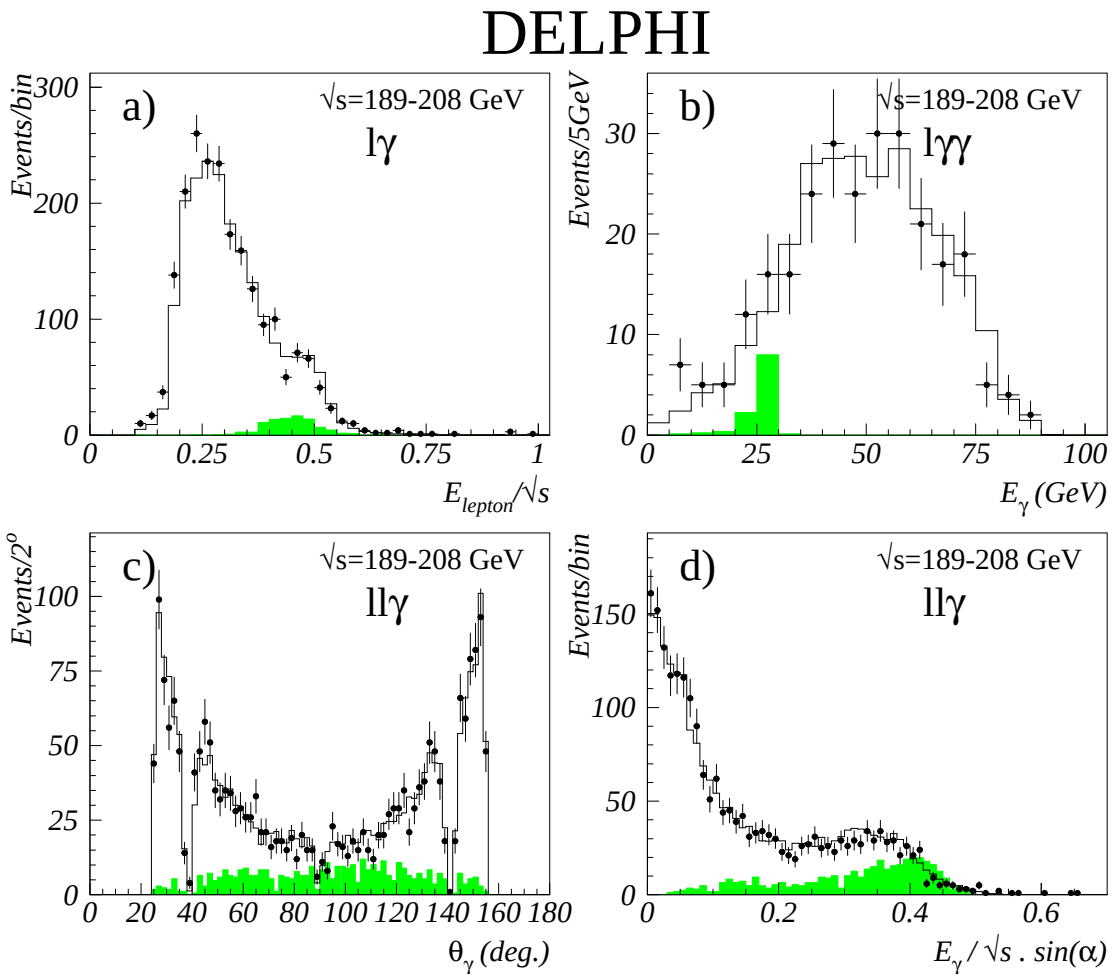

Figure 3: Topologies with leptons and photons after the preselection cuts: **(a)** Lepton energy in the $\ell\gamma$ topology; **(b)** Energy of the least energetic photon in the $\ell\gamma\gamma$ topology. **(c)** Photon polar angle and **(d)** $E_\gamma/\sqrt{s}\cdot\sin\alpha$, where α is the minimum angle between the photon direction and the two lepton directions, in the $\ell\ell\gamma$ topology. The dots show the data and the white histograms show the SM simulation. The shaded histograms show the expected distributions for a $m_{l^*} = 175$ GeV/c^2 excited lepton at $\sqrt{s} = 206$ GeV, using an arbitrary normalization.

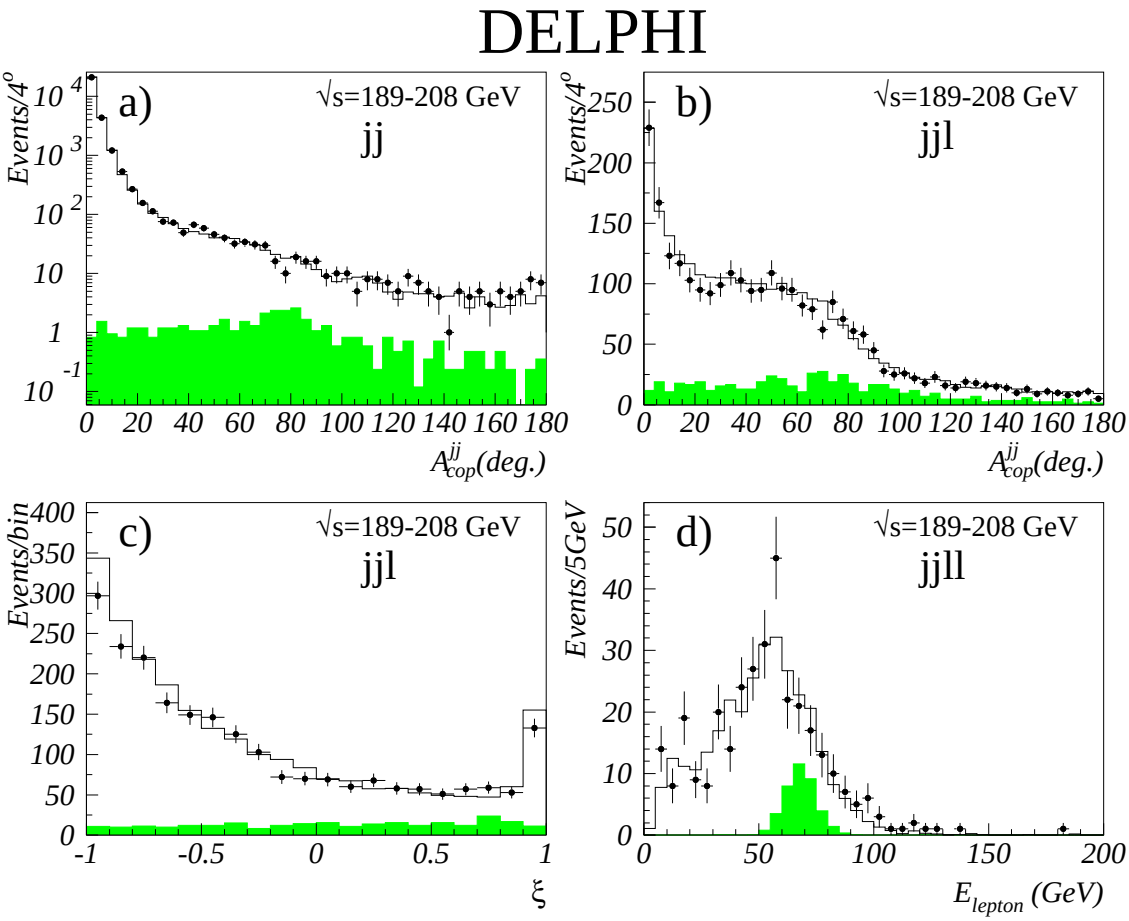

Figure 4: Topologies with jets and leptons after the preselection cuts: jet-jet acoplanarity in the jj **(a)** and $jj\ell$ **(b)** topologies; the variable $\xi = \mathrm{Q_W} \cdot \cos\theta_\mathrm{W}$ in the $jj\ell$ topology for events with the lepton charge unambiguously determined **(c)**; energy of the most energetic lepton for $jj\ell\ell$ events **(d)**. The dots show the data and the white histograms show the SM simulation. The shaded histograms show the expected distributions for a $m_{l^*} = 175$ GeV/c^2 excited lepton at $\sqrt{s} = 206$ GeV, using an arbitrary normalization.

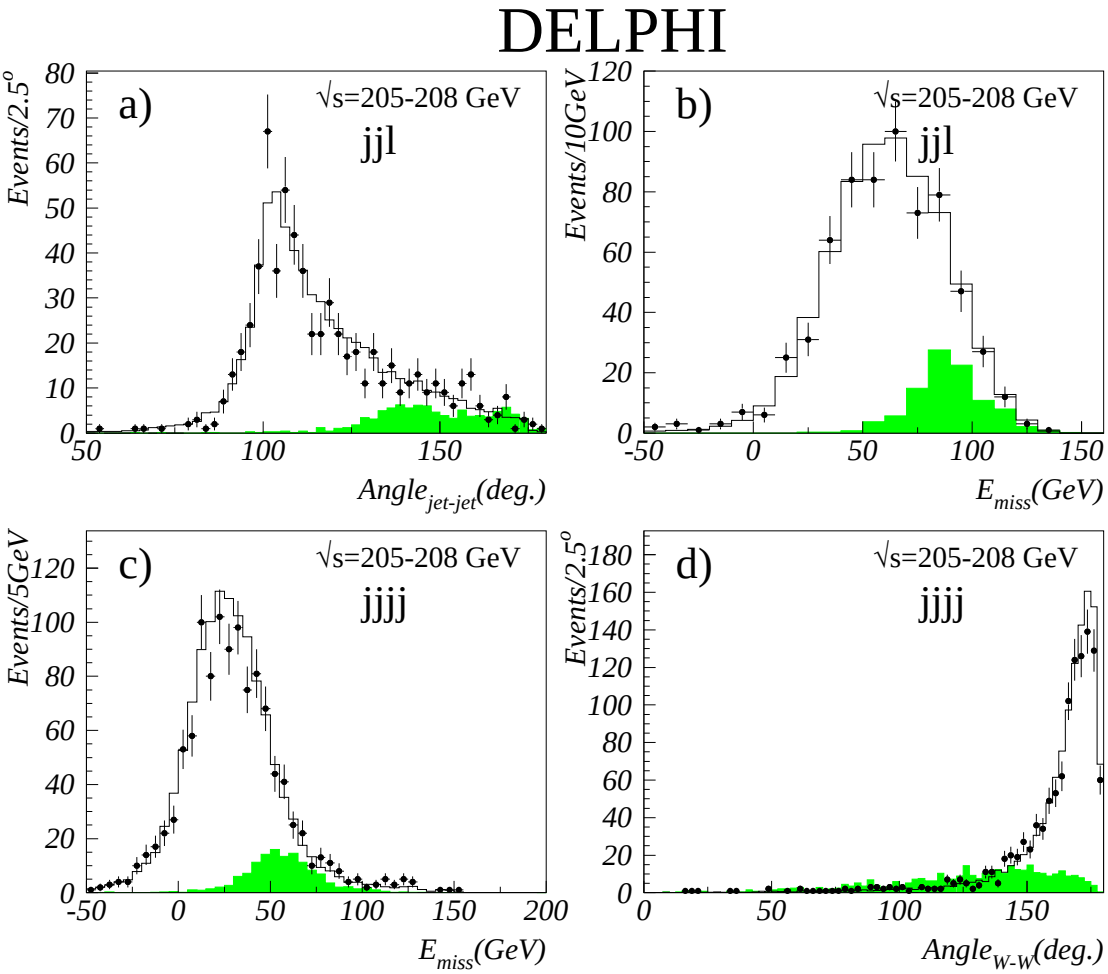

Figure 5: $\ell^*\ell^*$ search at the preselection level: **(a)** angle between the two jets and **(b)** missing energy in the semileptonic channel; **(c)** missing energy and **(d)** angle between the two reconstructed Ws in the fully hadronic channel. The dots show the data and the white histograms show the expected SM background. The shaded histograms show the expected signal distributions at $\sqrt{s} = 206$ GeV with m_{ℓ^*}=100 GeV/c^2, using an arbitrary normalization.

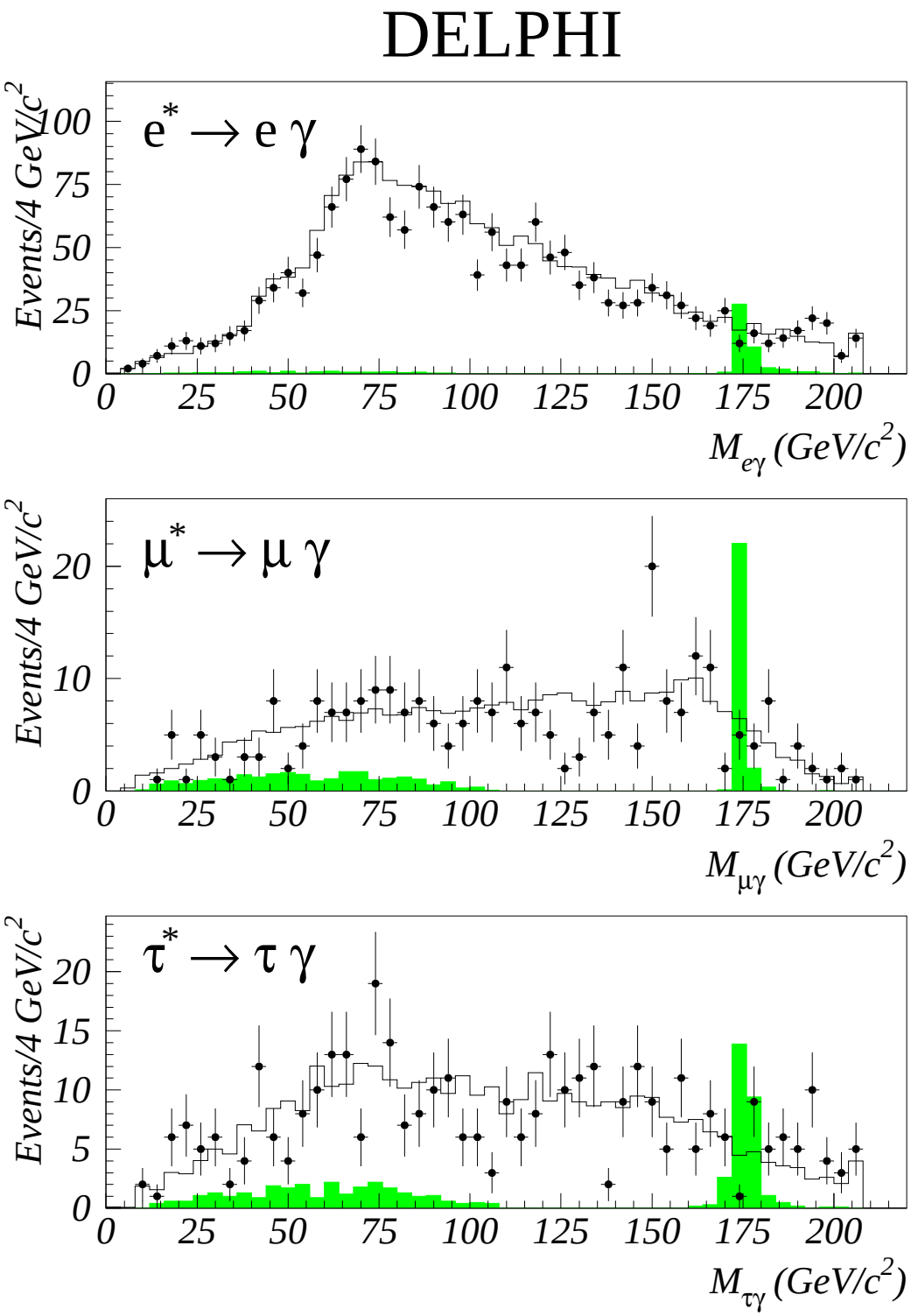

Figure 6: Lepton-photon invariant masses for the selected candidates in the $\ell^* \to \ell\gamma$ channels. Events selected in all relevant final state topologies at all centre-of-mass energies were added. For events from the $\ell\ell\gamma$ final state topology the two possible $\ell\gamma$ combinations are shown. The dots show the data and the white histograms show the expected SM background. The shaded histograms show the expected signal distributions at $\sqrt{s} = 206$ GeV with m_{l^*}=175 GeV/c^2, using an arbitrary normalization.

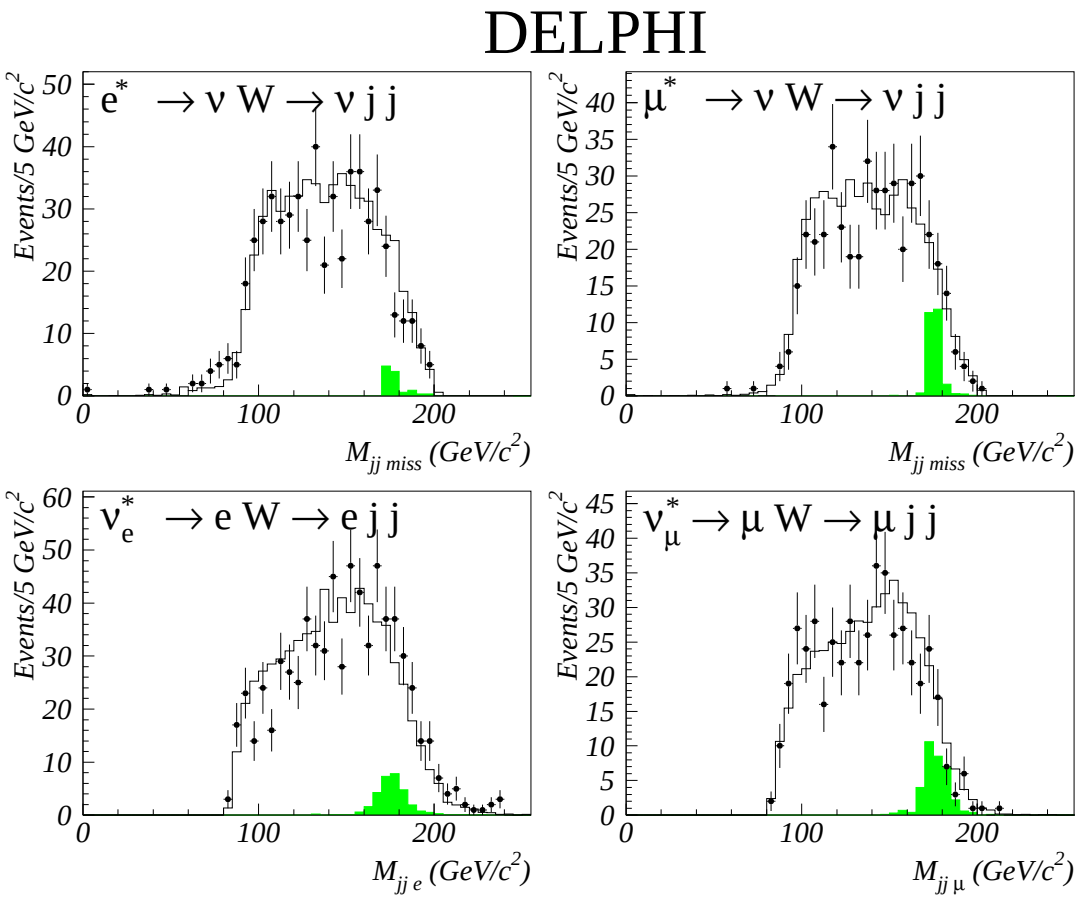

Figure 7: Invariant mass distributions for the selected candidates in the $\ell^* \to \nu W$ (top) and $\nu^* \to \ell W$ (bottom) channels. Events selected in the $jj\ell$ topology at all centre-of-mass energies were added. The dots show the data and the white histograms show the expected SM background. The shaded histograms show the expected signal distributions at $\sqrt{s} = 206$ GeV with m_{l^*}=175 GeV/c^2, using an arbitrary normalization.

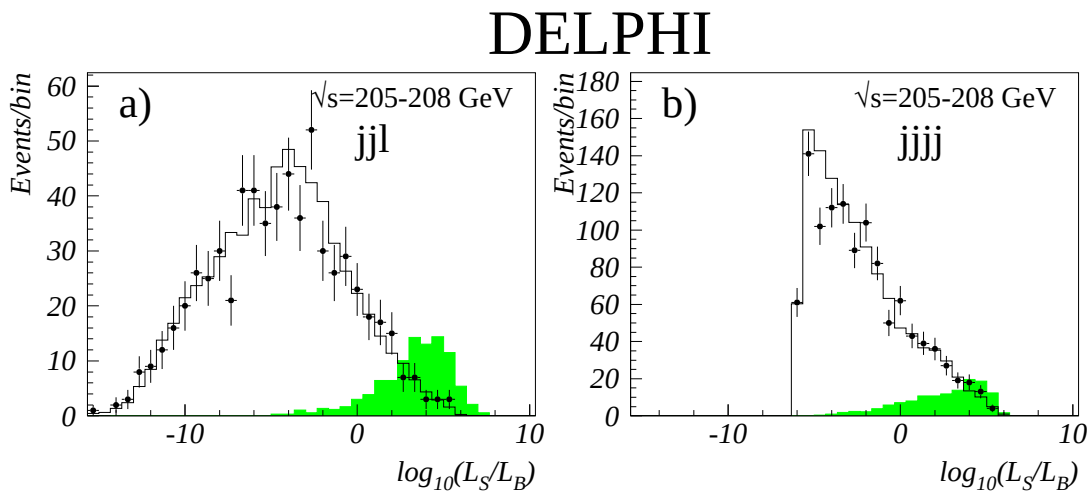

Figure 8: $\ell^*\ell^*$ search: discriminant variables in the **(a)** semileptonic and **(b)** fully hadronic channels. The dots are the data and the white histograms show the SM background expectation. The shaded histograms are the expected distributions for a m_{l^*}=100 GeV/c^2 signal at $\sqrt{s} = 206$ GeV, using an arbitrary normalization.

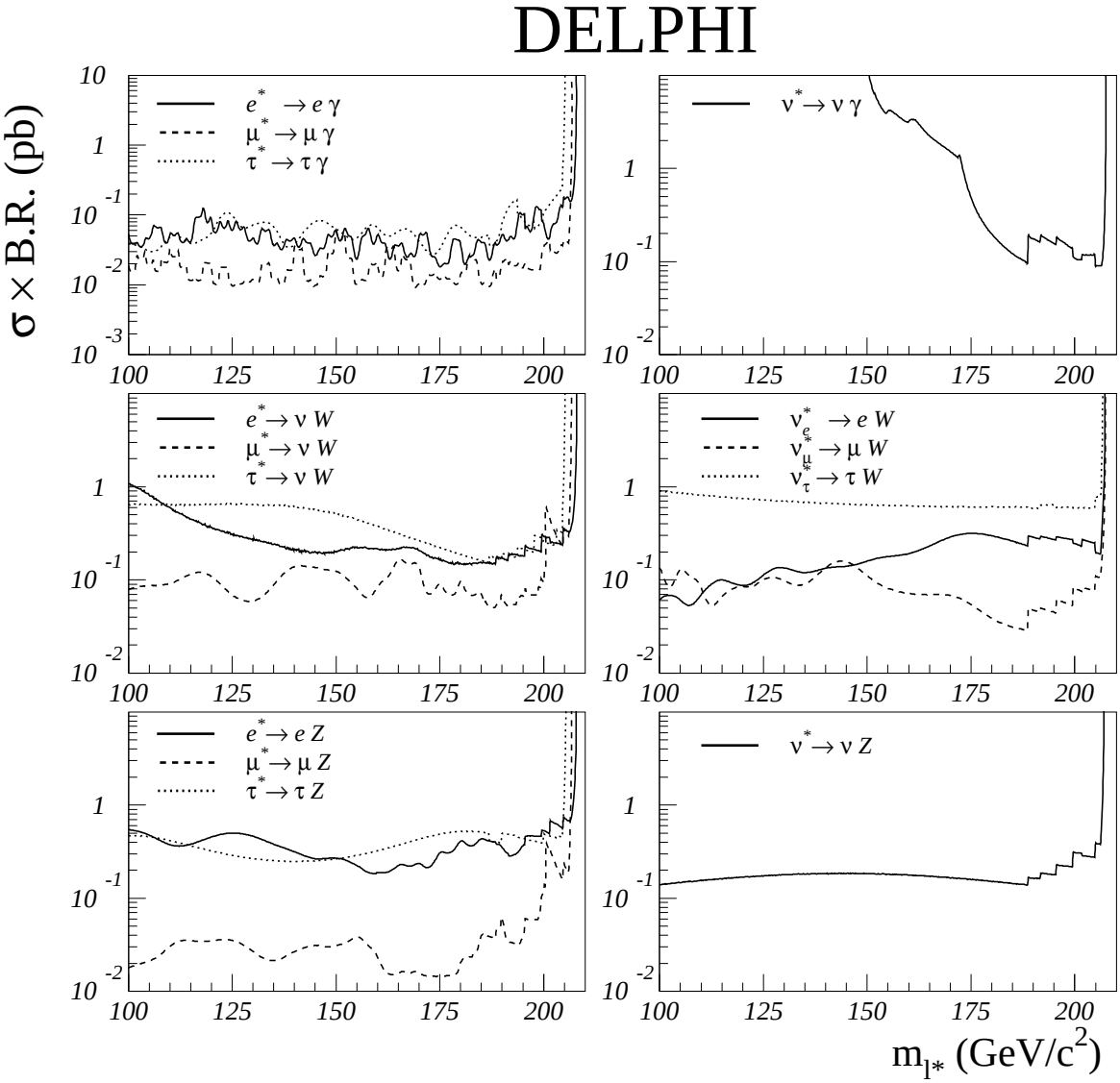

Figure 9: Results on the single production of charged and neutral excited leptons. The lines show the upper limits at 95% CL on $\sigma \times$ BR as a function of the particle mass, for each lepton flavour and decay mode.

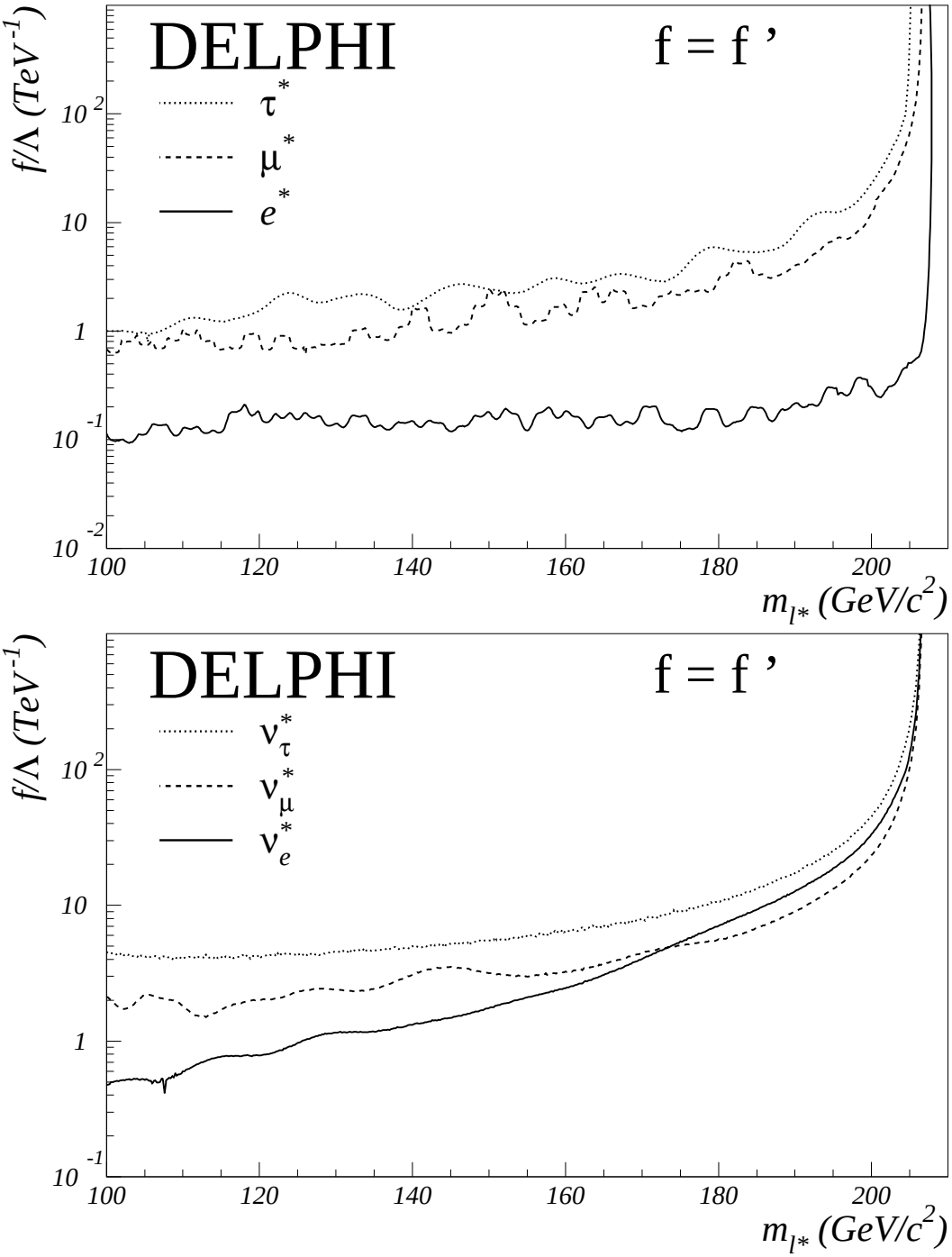

Figure 10: Results on single production of excited charged (upper plot) and neutral (lower plot) leptons assuming $f = f'$. The lines show the upper limits at 95% CL on f/Λ as a function of the excited lepton mass.

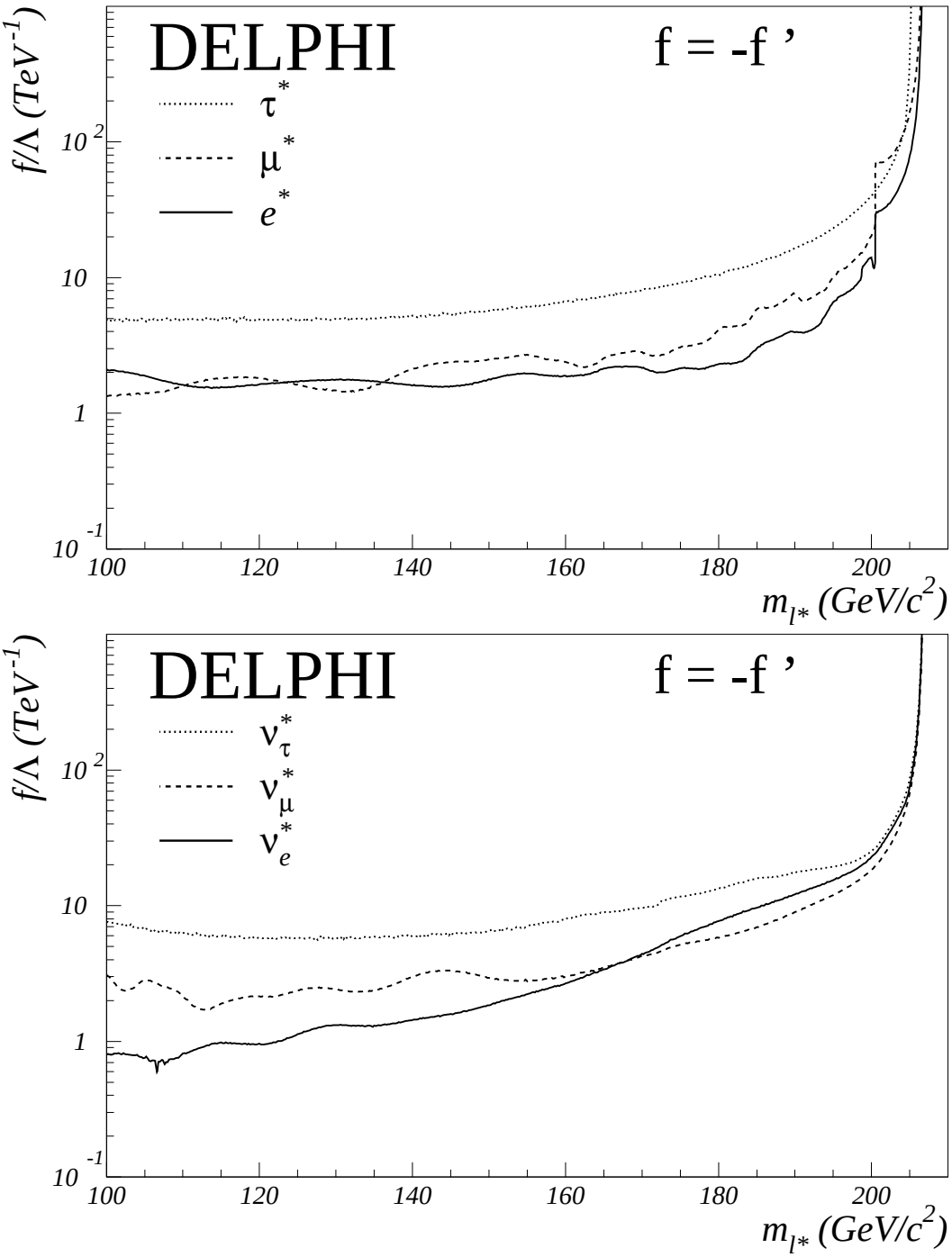

Figure 11: As figure 10, but for $f = -f'$.

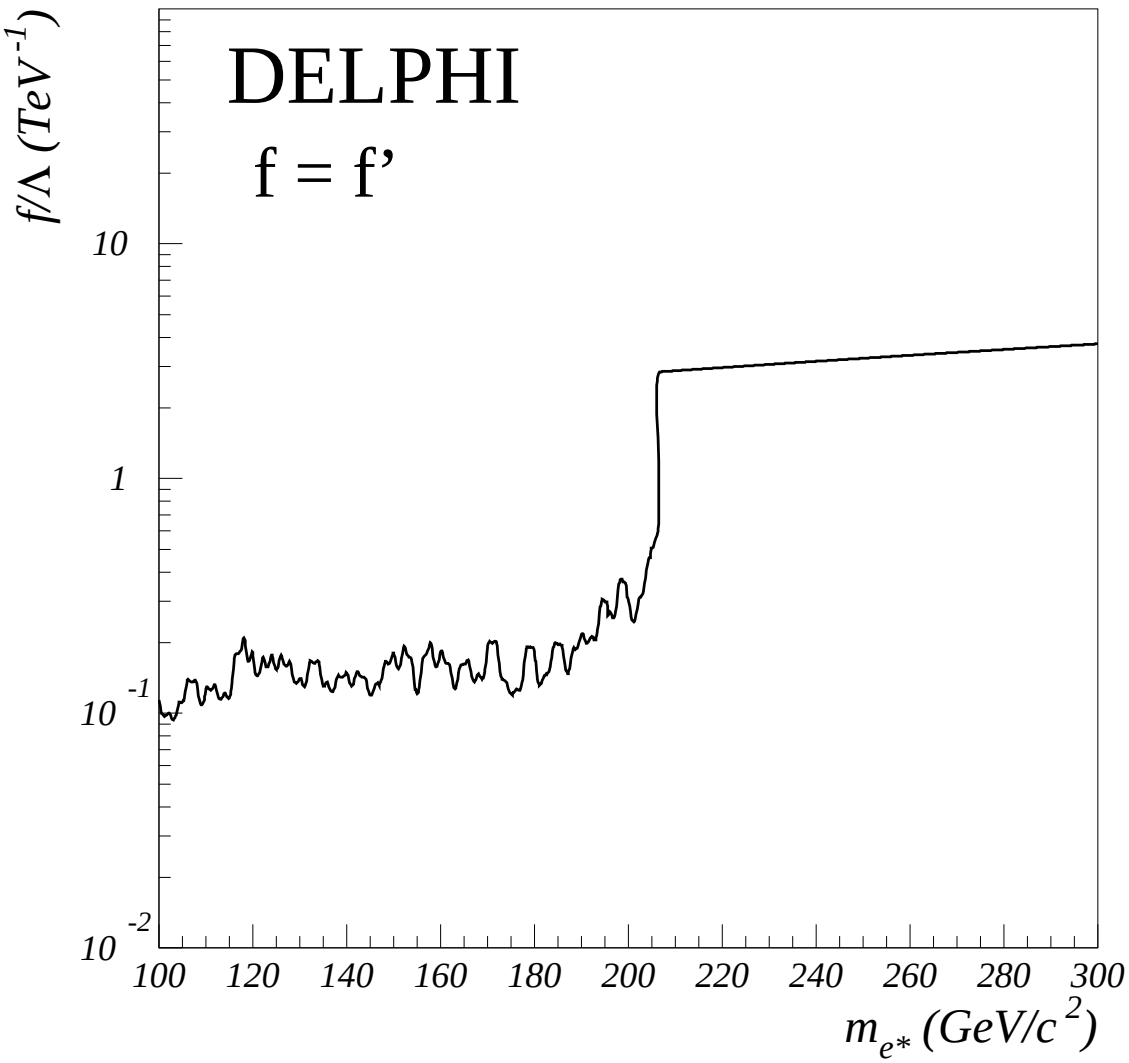

Figure 12: Combined limit on excited electron production for $f = f'$ from direct and indirect searches. The line shows the upper limit at 95% CL on f/Λ. Up to the kinematic limit the result is dominated by the direct search for single production. For masses above the kinematic limit the result stems from the indirect search of excited electron contribution to the process $e^+e^- \to \gamma\gamma$ as described in reference [8].